

SOC-DGL: Social Interaction Behavior Inspired Dual Graph Learning Framework for Drug-Target Interaction Identification

Xiang Zhao , Ruijie Li , *Student Member, IEEE*, Qiao Ning , Shikai Guo , Hui Li  and Qian Ma

Abstract—The identification of drug-target interactions (DTI) is crucial for drug discovery and repositioning, as it reveals potential uses of existing drugs, aiding in the acceleration of the drug development process and reducing associated costs. Despite the similarity information in DTI is important, most models are limited to mining direct similarity information within homogeneous graphs, overlooking the potential yet rich similarity information in heterogeneous graphs. Inspired by real-world social interaction behaviors, we propose SOC-DGL, which comprises two specialized modules: the Affinity-Driven Graph Learning (ADGL) module and the Equilibrium-Driven Graph Learning (EDGL) module. The ADGL module adopts a comprehensive social interaction strategy, leveraging an affinity-enhanced global drug-target graph to learn both global DTI and the individual similarity information of drugs and targets. In contrast, the EDGL module employs a higher-order social interaction strategy, amplifying the influence of even-hop neighbors through an even-polynomial graph filter grounded in balance theory, enabling the indirect mining of higher-order homogeneous information. This dual approach enables SOC-DGL to effectively and comprehensively capture similarity information across diverse interaction scales within the affinity matrices and drug-target association matrices, significantly enhancing the model's generalization capability and predictive accuracy in DTI tasks. To address the issue of imbalance in drug-target

interaction datasets, this paper proposes an adjustable imbalance loss function that mitigates the impact of sample imbalance by adjusting the weight of negative samples and a parameter. Extensive experiments on four benchmark datasets demonstrate significant accuracy improvements achieved by SOC-DGL, particularly in scenarios involving data imbalance and unseen drugs or targets.

Index Terms—Drug-target interaction, affinity-driven graph learning, equilibrium-driven graph learning, data imbalance.

I. INTRODUCTION

DRUG repurposing, the strategy of applying approved medications to novel therapeutic indications, has gained prominence due to the stagnation in traditional drug discovery [1]. Drug-target interactions (DTI) are central to pharmacology, yet conventional drug discovery remains time-consuming, costly, and high-risk [2]. In contrast, repurposing seeks to identify new uses for existing drugs, significantly reducing the time and cost of drug development [3]. Consequently, computational models for drug-target interactions have emerged, utilizing previous experimental data to predict novel DTI strengths. With the expanding availability of biomedical data, artificial intelligence-based methods for drug repurposing have proliferated [4], primarily falling into two key categories: machine learning-based methods and increasingly popular network-based methods.

Predicting DTI typically involves mapping drug-target pairs to feature vectors and applying machine learning for classification [5]–[7]. However, machine learning-based methods are limited by the need for positive and negative samples and are susceptible to sample imbalance, which can introduce noise and reduce prediction accuracy. Network-based methods typically build homogeneous or heterogeneous biological networks, infer interactions from drug-drug similarity, target-target similarity, or DTI, and predict interactions via network reasoning [8]–[11]. Although network-based reasoning methods are effective to some extent, they primarily focus on direct interactions and fail to explore similarity information embedded in heterogeneous information networks.

To address this challenge, this study proposes a novel social interaction-inspired dual-enhanced graph reasoning mechanism, termed SOC-DGL, which integrates ADGL and EDGL for accurate and robust DTI prediction based on similarity information from diverse sources. The main contributions of this study are:

This work was supported in part by the National Natural Science Foundation of China under Grant 62302075, in part by Innovation Support Program for Dalian High Level Talents under Grant 2023RQ007, and in part by the Dalian Excellent Young Project under Grant 2022RY35. (*Xiang Zhao and Ruijie Li contributed equally to this work and should be considered co-first authors.*) (*Corresponding authors: Qiao Ning; Shikai Guo.*)

Xiang Zhao is with the College of Marine Electrical Engineering, Dalian Maritime University, Dalian 116026, China, and with the Dalian Key Laboratory of Artificial Intelligence, Dalian 116024, China (e-mail: zhaoxiang@dlmu.edu.cn).

Ruijie Li and Shikai Guo are with the Department of Information Science and Technology, Dalian Maritime University, Dalian 116026, China, and with DUT Artificial Intelligence Institute, Dalian 116024, China, and also with the Dalian Key Laboratory of Artificial Intelligence, Dalian 116024, China (e-mail: lrj_d@dlmu.edu.cn, shikai.guo@dlmu.edu.cn).

Qiao Ning is with the Department of Information Science and Technology, Dalian Maritime University, Dalian 116026, China, and with the School of Artificial Intelligence and Computer Science, Jiangnan University, Wuxi 214122, China, and also with the Key Laboratory of Symbolic Computation and Knowledge Engineering of Ministry of Education, Jilin University, Changchun 130012, China (e-mail: ningq669@jiangnan.edu.cn).

Hui Li and Qian Ma is with the Department of Information Science and Technology, Dalian Maritime University, Dalian 116026, China (e-mail: li_hui@dlmu.edu.cn; maqian@dlmu.edu.cn).

The source code and data for SOC-DGL are available for academic purposes at <https://github.com/Zhaoxiang0422/SOC-DGL>.

- Inspired by real-world social interactions, this study proposes two complementary modules, ADGL and EDGL. Based on ADGL, which is built upon an extensive social interaction framework to achieve global representation learning on affinity-enhanced drug-target networks, EDGL further incorporates balance theory and employs an even-polynomial graph filter to capture high-order even-hop neighbor relationships in the heterogeneous drug-target graph. These two modules work in a complementary manner, enabling a comprehensive exploration of homogeneous information for both drugs and targets across multiple interaction scales.
- To mitigate the impact of imbalanced data on the performance of SOC-DGL, this study designs a novel adjustable imbalance loss function that mitigates the impact of sample imbalance by weighting negative samples and introducing an adjustable parameter ϖ . Extensive experimental results on imbalanced benchmark datasets consistently demonstrate the effectiveness.
- ABL1, a key pathogenic target in Chronic Myeloid Leukemia, is effectively targeted by 10 drugs predicted by SOC-DGL. Utilizing a homogeneous information aggregation mechanism, SOC-DGL uncovers a potential association between Debromohymenialdisine and ABL1, highlighting its capability to identify novel DTI.

II. RELATED WORK

A. DTI Prediction Based on Similarity

The integration of similarity information plays a pivotal role in advancing DTI prediction models. Traditionally, similarity mining has focused on isomorphic networks, where pairwise similarity between drugs and targets is utilized [12]–[14]. However, recent work has shifted towards heterogeneous graphs, which integrate multiple types of nodes and relationships [15]–[17]. Despite these advancements, these approaches primarily rely on similarity information derived from traditional similarity matrices, overlooking the rich and potentially valuable indirect similarity information between drugs and targets embedded within heterogeneous graphs. Such higher-order similarity information is critical for predicting potential DTI associations and necessitates the design of specialized modules for its learning.

B. High-order Similarity Information Learning

Effectively learning high-order similarity information aids in uncovering complex higher-order isomorphic relationships in graph data. Mi et al. [18] proposed HSL, which learns high-order similarity by considering both first-order and high-order similarities in a low-dimensional embedding space. Wang et al. [19] introduced HSDA for speech emotion recognition, capturing high-order similarity through a similarity graph to reveal cross-domain structural relationships. Peng et al. [20] proposed HSC, where high-order similarity is learned from relationships between dimensional spaces and jointly optimized with ordinary similarity for clustering. Inspired by these methods and balance theory [21], we propose the EDGL module, built upon the ADGL module, to fully exploit high-order similarity information for DTI prediction.

III. DATASETS AND METHODOLOGY

A. Datasets

To comprehensively assess the performance and applicability of SOC-DGL, this study selects four representative benchmark datasets: KIBA [22], Davis [23], BindingDB [24], and DrugBank [25], whose detailed description appears in Appendix Section A.

B. Model framework overview

The framework of SOC-DGL is composed of six main steps, as shown in Fig. 1, including: (I) Affinity-Enhanced Global Drug-Target Network Construction, (II) Affinity-Driven Graph Learning, (III) Equilibrium-Driven Graph Learning, (IV) Feature Fusion, (V) DTI Prediction Decoder, and (VI) Imbalanced Processing.

1) *Affinity-Enhanced Global Drug-Target Network Construction*: In DTI prediction, diverse features of drugs and targets are derived from various measurement methods, offering complementary perspectives on molecular characteristics. Integrating these heterogeneous features is crucial for accurate DTI inference. Assuming a shared latent space for drug and target features, SOC-DGL employs pairwise multi-view learning to derive a unified subspace representation from multiple views, specifically the drug affinity matrix (A_{DD}) and target affinity matrix (A_{TT}). SOC-DGL effectively integrates multi-view information by constructing a protocol matrix that combines correlation matrices under low-rank and sparsity constraints. Details are provided in Appendix Section B.

The drug-target affinity matrix is denoted as A_{DT} . By combining A_{DD} , A_{TT} , and A_{DT} , this study constructs an affinity-enhanced global drug-target network matrix H , where A_{TD} is the transpose of A_{DT} , and H is a symmetric matrix:

$$H = \begin{pmatrix} A_{DD} & A_{DT} \\ A_{TD} & A_{TT} \end{pmatrix} \in \mathbb{R}^{(n_d+n_t) \times (n_d+n_t)} \quad (1)$$

2) *Affinity-Driven Graph Learning*: To extract both direct and global DTI and similarity information of drugs and targets, this study employs an extensive social interaction strategy and apply global graph convolutional learning to the affinity-enhanced global drug-target network matrix.

To effectively filter the useful information within the heterogeneous graph, for drug affinity matrix A_{DD} and the target affinity matrix A_{TT} , elements in these two affinity matrices that are greater than or equal to the threshold 0.8 are set to 1, and the rest are set to 0, resulting in the drug affinity adjacency matrix \tilde{A}_{DD} and the target affinity adjacency matrix \tilde{A}_{TT} . By combining the drug-target affinity matrix, this study constructs the adjacency matrix G of:

$$G = \begin{pmatrix} \tilde{A}_{DD} & A_{DT} \\ A_{TD} & \tilde{A}_{TT} \end{pmatrix} \in \mathbb{R}^{(n_d+n_t) \times (n_d+n_t)} \quad (2)$$

Subsequently, this study performs graph convolution operations:

$$H^{(l+1)} = \sigma(D^{-\frac{1}{2}}GD^{-\frac{1}{2}}H^{(l)}W^{(l)}) \quad (3)$$

where $D^{-1/2}GD^{-1/2}$ represents the normalization process, with $D = \text{diag}(\sum_j G_{ij})$ being the degree matrix of the

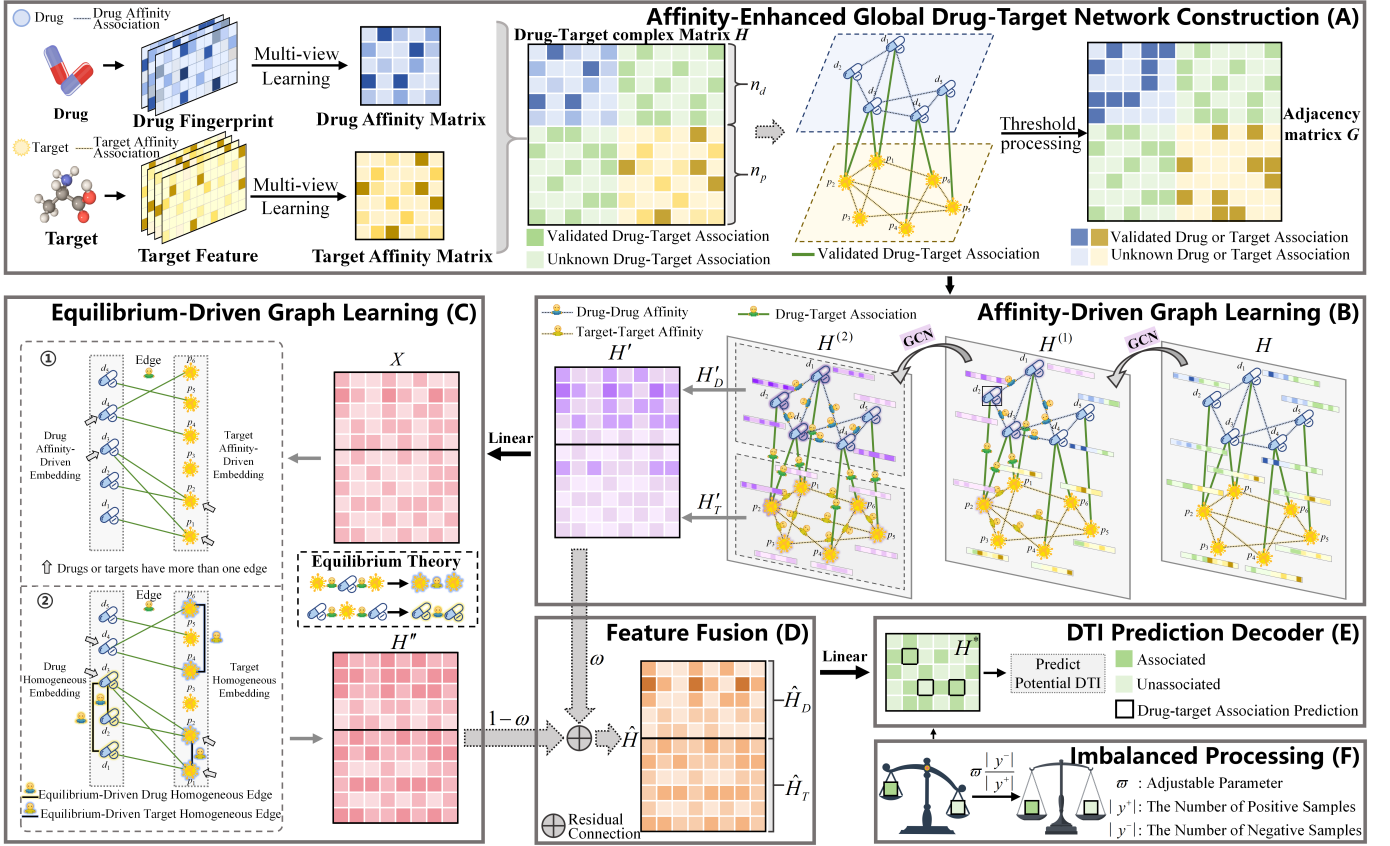


Fig. 1: The framework of SOC-DGL. (A) Affinity-enhanced global drug-target network construction, (B) Affinity-Driven Graph Learning, (C) Equilibrium-Driven Graph Learning, (D) Feature fusion, (E) DTI prediction decoder, and (F) Imbalanced Processing.

adjacency matrix G . $H^{(l)}$ is the feature embedding matrix at layer l , $W^{(l)}$ is the learnable weight matrix at layer l , and σ is the activation function. After two rounds of graph convolution, the graph convolution feature embedding matrix H' is obtained:

$$H' = \begin{bmatrix} H'_D \\ H'_T \end{bmatrix} \in \mathbb{R}^{(n_d+n_t) \times m} \quad (4)$$

where $H'_D \in \mathbb{R}^{n_d \times m}$ is the drug feature embedding matrix, $H'_T \in \mathbb{R}^{n_t \times m}$ is the target feature embedding matrix, and m is the final output dimension.

3) Equilibrium-Driven Graph Learning: In the real situation, drugs with similar structures may exhibit analogous mechanisms of action, while the similarity between targets reflects the functional conservation of targets [26]. As the classic adage goes: “The friend of my friend is also my friend,” this concept is equally applicable to DTI. Using balance theory [21], this study deduces that even though drugs and targets differ in their attributes, they can establish connections through shared interaction relationships. If a drug interacts with multiple targets, and these targets are connected to other drugs, then these drugs and targets may form a state of equilibrium through these indirect interaction relationships. To this end, this study proposes the EDGL module, which employs a higher-order social interaction strategy to indirectly learn higher-order drug and target similarity information linked by ‘friend nodes’ through an even-polynomial graph filter.

This study processes H' , which has been encoded through ADGL. For ease of expression, let $X_0 = H'$, and then perform two linear transformations on X_0 , applying an activation function. X is obtained as follows:

$$X_{(l+1)} = \sigma(X_{(l)} \cdot W_{(l)} + b_{(l)}) \quad (5)$$

This study normalizes the adjacency matrix G by setting $G' = D^{-1/2}GD^{-1/2}$, where D is the degree matrix of the adjacency matrix G . Thus,

$$G' = \begin{pmatrix} \tilde{A}'_{DD} & \tilde{A}'_{DT} \\ \tilde{A}'_{TD} & \tilde{A}'_{TT} \end{pmatrix} \in \mathbb{R}^{(n_d+n_t) \times (n_d+n_t)} \quad (6)$$

To learn similarity information in drug-target association matrix, this study sets $(\tilde{A}'_{DD})_{ij} = 0$, $(\tilde{A}'_{TT})_{ij} = 0$, thereby transforming it into the adjacency matrix A' :

$$A' = \begin{pmatrix} 0 & \tilde{A}'_{DT} \\ \tilde{A}'_{TD} & 0 \end{pmatrix} \in \mathbb{R}^{(n_d+n_t) \times (n_d+n_t)} \quad (7)$$

where $A'_{DP} \in \mathbb{R}^{n_d \times n_t}$, $\tilde{A}'_{DD} \in \mathbb{R}^{n_d \times n_d}$. This study then obtains the Laplacian matrix $L = D' - A'$, where D' is the degree matrix of L . After standardizing L , the formula is as follows:

$$\tilde{L} = D'^{-\frac{1}{2}}LD'^{-\frac{1}{2}} = I - D'^{-\frac{1}{2}}A'D'^{-\frac{1}{2}} \quad (8)$$

where I is the identity matrix. Subsequently, this study defines the propagation matrix as $P = I - \tilde{L} = D^{-1/2}A'D^{-1/2}$, and

the k -th order polynomial graph filter is defined as $g(\tilde{L}) = \sum_{k=0}^K \alpha_k \tilde{L}^k$, $k = 0, 1, \dots, K$, where α_k is the learnable weight matrix, and $\alpha_k = \alpha \times (1 - \alpha)^k$, with α being a hyperparameter that can be set. Thereafter, this study rewrites the graph filter formula as $g(\tilde{L}) = \sum_{k=0}^K \alpha_k (I - \tilde{L})^k = \sum_{k=0}^K \alpha_k P^k$, discarding the odd-degree terms in $g(\tilde{L})$ and retaining only even-degree terms:

$$g_{\text{even}}(\tilde{L}) = \sum_{k=0}^{\lfloor \frac{K}{2} \rfloor} \alpha_{2k} (I - \tilde{L})^{2k} = \sum_{k=0}^{\lfloor \frac{K}{2} \rfloor} \alpha_k P^{2k} \quad (9)$$

Thus, the model of EDGL is constructed:

$$Y = f(\hat{X}, P) = \sum_{k=0}^{\lfloor \frac{K}{2} \rfloor} \alpha_k P^{2k} \hat{X} \quad (10)$$

where \hat{X} is the input feature matrix that has already undergone two linear transformations, and Y represents the final output features. This study denotes the result obtained after passing H' through EDGL as H'' , and its expression is as follows:

$$H'' = Y = \begin{bmatrix} H''_D \\ H''_T \end{bmatrix} \in \mathbb{R}^{(n_d+n_t) \times m} \quad (11)$$

4) Feature Fusion: This study employs residual connection techniques to integrate information from diverse sources, ensuring that the two modules complement each other and collectively form a more powerful graph reasoning mechanism. "This approach balances the influence of higher-order interaction patterns on the generalized patterns, achieving equilibrium between the two "social interaction paradigms." The corresponding formula is as follows:

$$\hat{H} = \omega H' + (1 - \omega) H'' \quad (12)$$

where ω represents the weight, which is an adjustable hyperparameter. The integrated features \hat{H} will serve as the input for the decoder, used to predict DTI. Through residual connection feature fusion, this study gains a multifaceted understanding of the complex relationships between drugs and targets.

5) DTI prediction decoder: DTI prediction decoder in SOC-DGL cleverly employs the principle of matrix factorization. By meticulously decoding these features, it reveals the affinity between drugs and targets, assessing the potential interaction affinity between different drugs and targets. This study denotes W^L as the learnable weight matrix for the mapping from the drug space to the target space within the decoder. Inspired by matrix tri-factorization, the formula for DTI prediction decoder is as follows:

$$H^* = \sigma(\hat{H}_D W^{(L)} \hat{H}_P^T) \quad (13)$$

where H^* represents the final predicted interaction matrix, and its element H^*_{ij} denotes the predicted association score between drug i and target j .

6) Imbalanced Processing: To address the issue of class imbalance between positive and negative samples in the model, this study designs a Weighted Binary Cross-Entropy Loss Function with Reduced Regative Samples (RLF), as shown in the following formula:

$$\mathcal{L} = -\frac{1}{n_d \cdot n_t} \left(\varpi \frac{|y^-|}{|y^+|} \sum_{(i,j) \in y^+} \log(h^*_{ij}) + \sum_{(i,j) \in y^-} \log(1 - h^*_{ij}) \right) \quad (14)$$

where n_d is the number of drugs, n_t is the number of targets, $|y^+|$ represents the number of positive samples, and $|y^-|$ represents the number of negative samples. h^*_i represents the model's predicted probability of interaction between drug i and target j . This novel loss function is built upon the existing weighted cross-entropy loss function, with the introduction of an adjustable parameter ϖ , which effectively reduces the weights of negative samples while keeping the weights of positive samples unchanged.

IV. EXPERIMENTS AND RESULTS

A. Experimental design overview

In the "warm-start" scenario, this study designed validation experiments for both balanced datasets (positive:negative samples = 1:1) and imbalanced datasets (positive:negative samples = 1:10). In most real-world tasks, the ratio of positive to negative samples is typically imbalanced. In drug-target association prediction, known associations (positive samples) were generally far fewer than unknown associations (negative samples). Evaluating with imbalanced datasets better reflected SOC-DGL's performance in real-world settings. Conversely, balancing the positive and negative samples helped mitigate model bias towards predicting negative samples, providing a more balanced assessment of model performance.

To minimize the impact of data variability on the results, this study employed 10-fold cross-validation to assess the model's predictive performance. First, the entire dataset (positive and negative samples) was randomly divided into 10 subsets of approximately equal size. This process was repeated 10 times, with each time selecting a different subset as the test set and the other 9 subsets as the training set. Initially, the test set data was masked, and then the model was trained on the remaining 9 subsets. The masked test set values were predicted for DTI, and the predicted values were compared with the actual DTI values (before masking) using the AUROC, AUPR, F1_score, Accuracy (ACC), Recall, Specificity, and Precision metrics.

In this study, in the "warm-start" scenario, comprehensive experimental validation was conducted on four representative benchmark datasets to assess the performance of SOC-DGL. For other specific experiments, the study primarily chose to conduct validation on the KIBA dataset due to its moderate data size and comprehensive information, which provided accurate support for model training and evaluation.

This study conducted experiments using PyTorch 1.11.0 on an Nvidia GeForce RTX 3060 GPU, and employed the Xavier initialization strategy to prevent gradient explosion and vanishing during the training process.

TABLE I: SOC-DGL performance in the “warm-start” scenario on four benchmark datasets.

Dataset	KIBA dataset		Davis dataset		BindingDB dataset		DrugBank dataset	
	balanced	imbalanced	balanced	imbalanced	balanced	imbalanced	balanced	imbalanced
AUROC	0.9761 ± 0.0023	0.9364 ± 0.0036	0.9467 ± 0.0074	0.9192 ± 0.0045	0.9894 ± 0.0032	0.9790 ± 0.0034	0.9735 ± 0.0023	0.9295 ± 0.0076
AUPR	0.9805 ± 0.0018	0.7473 ± 0.0123	0.9673 ± 0.0048	0.7655 ± 0.0134	0.9888 ± 0.0036	0.8705 ± 0.0146	0.9774 ± 0.0019	0.7654 ± 0.0126
F1_score	0.9350 ± 0.0041	0.6908 ± 0.0068	0.9038 ± 0.0103	0.6918 ± 0.0129	0.9641 ± 0.0075	0.8057 ± 0.0177	0.9286 ± 0.0027	0.7211 ± 0.0104
ACC	0.9268 ± 0.0049	0.9207 ± 0.0026	0.8816 ± 0.0131	0.9134 ± 0.0030	0.9627 ± 0.0077	0.9594 ± 0.0041	0.9267 ± 0.0026	0.9508 ± 0.0015
Recall	0.9373 ± 0.0093	0.7103 ± 0.0182	0.9097 ± 0.0200	0.6642 ± 0.0338	0.9677 ± 0.0098	0.8406 ± 0.0246	0.9208 ± 0.0136	0.6567 ± 0.0210
Specificity	0.9133 ± 0.0148	0.9506 ± 0.0049	0.8372 ± 0.0362	0.9561 ± 0.0066	0.9574 ± 0.0107	0.9726 ± 0.0047	0.9331 ± 0.0130	0.9824 ± 0.0022
Precision	0.9328 ± 0.0100	0.6730 ± 0.0177	0.8985 ± 0.0189	0.7238 ± 0.0230	0.9606 ± 0.0097	0.7744 ± 0.0304	0.9369 ± 0.0109	0.8004 ± 0.0174

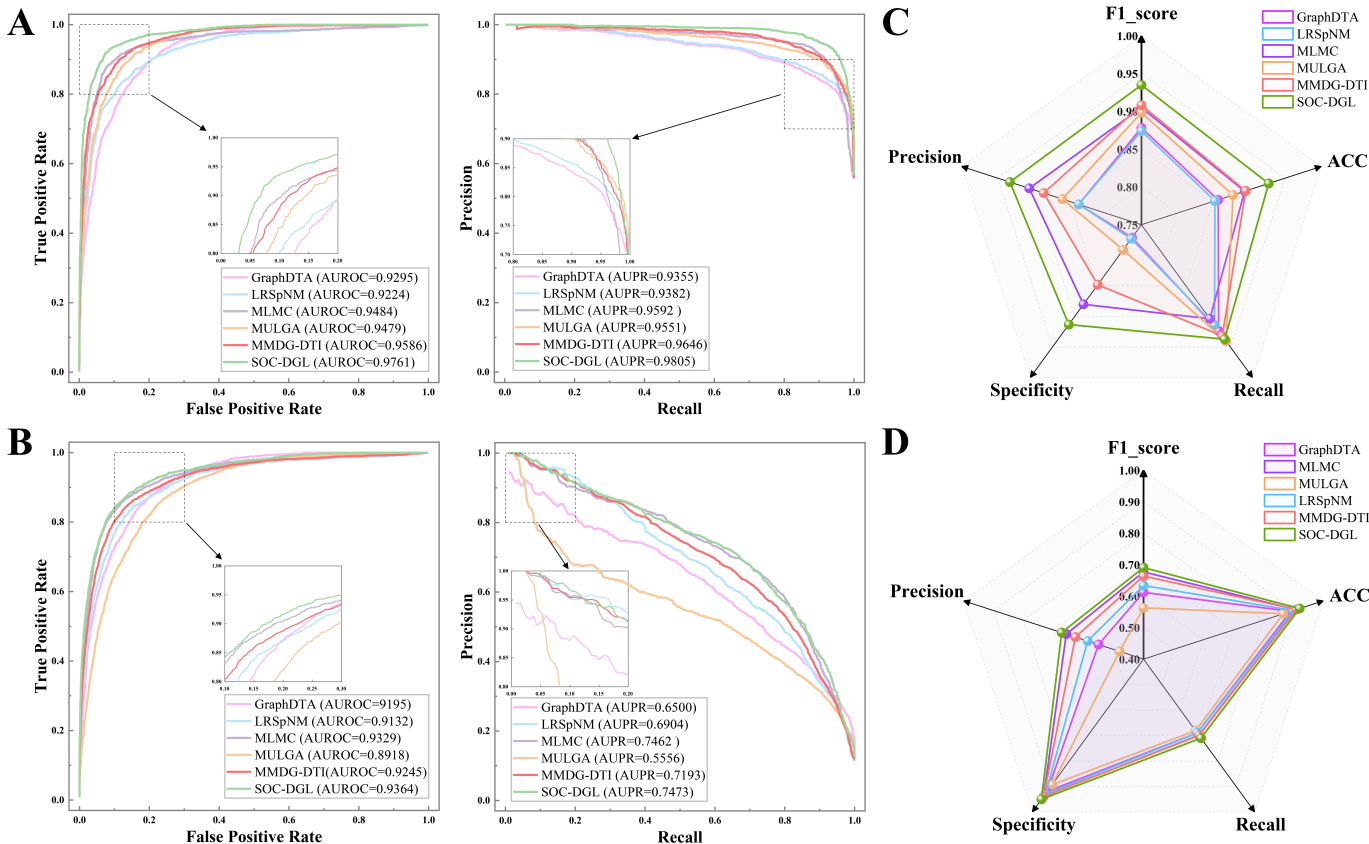


Fig. 2: Performance comparison of SOC-DGL with baseline methods on the KIBA dataset. (A) ROC and PR curves on balanced datasets and (B) imbalanced datasets. (C) F1 score, ACC, recall, specificity, and precision on balanced datasets and (D) imbalanced datasets.

B. “Warm-start” experiments

In this study, “Warm-start” experiments were conducted on four benchmark datasets under both balanced and imbalanced settings. Multiple runs were performed on each dataset with optimized parameter configurations, and average metrics with standard deviations were reported, as shown in Tab. I. The results demonstrated that SOC-DGL achieved high predictive accuracy in balanced settings, effectively distinguishing known DTIs, and performed well in the “warm-start” scenario, validating application in DTI prediction and drug discovery.

To assess SOC-DGL’s effectiveness, comparative experiments were conducted with four leading DTI prediction methods: GraphDTA [27], LRSpNM [28], MLMC [29], MULGA [30], and MMDG-DTI [31], representing the state-of-the-art. Detailed comparisons were available in Appendix Section C. SOC-DGL showed significant improvements on both balanced and imbalanced datasets, demonstrating its

broad applicability and outperformance over current methods.

As shown in Fig. 2(A) and Fig. 2(B), SOC-DGL consistently outperformed all baseline methods on both balanced and imbalanced datasets. It was clearly evident that MMDG-DTI consistently performed just slightly behind SOC-DGL on the KIBA balanced dataset. MLMC also showed strong performance, leveraging multi-view learning and matrix completion techniques. In contrast, LRSpNM, based on low-rank matrix approximation, performed the worst across all datasets, likely due to DPI matrix sparsity and inaccurate similarity measures. On the KIBA balanced dataset, SOC-DGL’s AUROC and AUPR were 1.8% and 1.6% higher compared to the current best-performing model, respectively, and 0.4% and 0.1% higher in the imbalanced setting. MLMC and MULGA performed slightly worse than SOC-DGL, with MULGA underperforming in imbalanced settings due to inadequate attention to homogeneous association information. However, in other datasets, MULGA’s multi-view learning

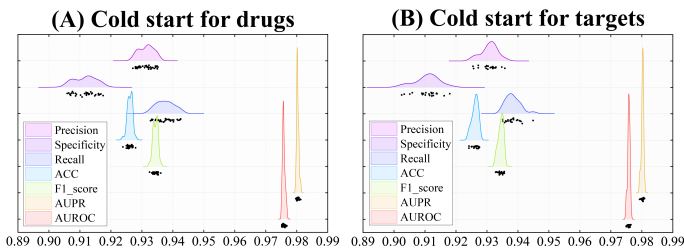


Fig. 3: Performance scores of SOC-DGL in "cold-start" scenarios for drugs and targets, evaluated on various metrics. Black dots represent randomly sampled data points corresponding to indicator values of these metrics.

approach combined with graph autoencoders ranked second to SOC-DGL, suggesting lower generalizability. Appendix Tab. I further confirmed SOC-DGL's superiority across datasets. The F1-score, ACC, Recall, Specificity, and Precision results in Fig. 2(C) and Fig. 2(D) further validated SOC-DGL's consistent outperformance.

C. "Cold-start" experiments

In the "cold-start" experiments on the KIBA dataset, two scenarios were designed: "cold-start for drugs" and "cold-start for targets," where the drug-target affinity matrix was systematically sampled. In the "cold-start for targets" scenario, drugs linked to specific targets were removed, treating each target as new, with the removed data serving as the test set. In the "cold-start for drugs" scenario, drugs linked to specific targets were removed, and the corresponding test set consisted of the removed drugs and their targets.

The KIBA dataset, comprising 1,720 drugs and 220 targets, provided the foundation for "Cold-start" experiments. A total of 56 independent cold-start experiments were conducted, involving the random selection of 34 drugs and 22 targets to simulate real-world scenarios where new drugs or targets lacked historical interaction data. This was particularly relevant in drug discovery, where novel compounds or under-explored proteins often lacked prior interaction data.

Fig. 3 presented the results. In the "cold-start for drugs" scenario, SOC-DGL showed stable performance across different drugs, with an average AUROC of 0.9758 and AUPR of 0.9803, indicating strong generalization ability for new drugs. Similarly, in the "cold-start for targets" scenario, SOC-DGL demonstrated consistent performance across different targets. These results confirmed its robustness in predicting drug-target interactions for unseen drugs or targets, making it a valuable tool for practical drug development and target discovery.

D. Analysis of the Even-Polynomial Graph Filter in EDGL

To analyze the importance of the even-polynomial graph filter in EDGL for indirectly extracting higher-order homogeneous information between drugs and targets, this study compared it with the odd-polynomial graph filter for indirectly extracting higher-order heterogeneous information and with the self-attention mechanism under the "warm start" scenario, while keeping all other modules unchanged. Specifically, this study evaluated the effectiveness of higher-order similarity

information enhancement by the even-polynomial graph filter (Homogeneous_prop), higher-order interaction information enhancement by the odd-polynomial graph filter (Heterogeneous_prop), and self-information enhancement by the self-attention mechanism (Self_attention_prop) using various metrics to comprehensively measure their performance.

As shown in Fig. 4(A), Homogeneous_prop outperformed Heterogeneous_prop and Self_attention_prop, particularly in AUROC and AUPR, excelling in DTI prediction and handling imbalanced data by capturing complex indirect relationships. While Heterogeneous_prop was effective for direct connections, it struggled with indirect ones. Self_attention_prop, despite its node-weighting capability, performed weaker overall in managing complex interactions. Homogeneous_prop showed a trade-off with slightly lower Recall, indicating reduced sensitivity to some positives. These results highlighted the superior ability of Homogeneous_prop to capture indirect interactions and improve prediction accuracy.

E. Ablation Study on Diversity Graph Learning

To evaluate the impact of different graph learning modules, three SOC-DGL variants were tested: (1) ADGL-Only, focusing on global associations, (2) EDGL-Only, emphasizing higher-order similarities, and (3) Fusion-Without, combining the two modules without feature fusion residual connection to assess the role of feature fusion.

As shown in Fig. 4 (B), SOC-DGL outperformed the variants on most metrics, particularly in AUROC and AUPR. On balanced datasets, SOC-DGL achieved an AUROC of 0.9761, surpassing ADGL-Only (0.9660) and EDGL-Only (0.9703), demonstrating the clear benefit of combining ADGL and EDGL for capturing complex DTIs. Similarly, SOC-DGL's AUPR of 0.9805 exceeded ADGL-Only (0.9707) and EDGL-Only (0.9690). While Fusion-Without showed comparable performance in some cases, it fell short overall, indicating that the residual fusion method, which effectively balanced the importance of different DTI patterns, more effectively identified and integrated complex interaction pathways, thereby improving model generalization.

F. Validation Experiment on Imbalanced Loss Function

In DTI prediction, there was often an imbalance between positive and negative samples, which could affect model performance, causing it to favor the majority class while neglecting the minority. This experiment evaluated the impact of various loss functions on model performance, focusing on those designed to address class imbalance.

Four loss functions were assessed: Standard Binary Cross-Entropy Loss (SLF), Focal Loss with Dynamic Scaling (FLF), Weighted Binary Cross-Entropy Loss (WLF), and Weighted Binary Cross-Entropy Loss with Reduced Negative Samples (RLF). Experiments were conducted in a "warm-start" scenario with imbalanced datasets, evaluating DTI prediction performance across multiple metrics. Details of these loss functions could be found in Appendix Section E.

As shown in Tab. II, the RLF loss function consistently outperformed the others across four benchmark imbalanced

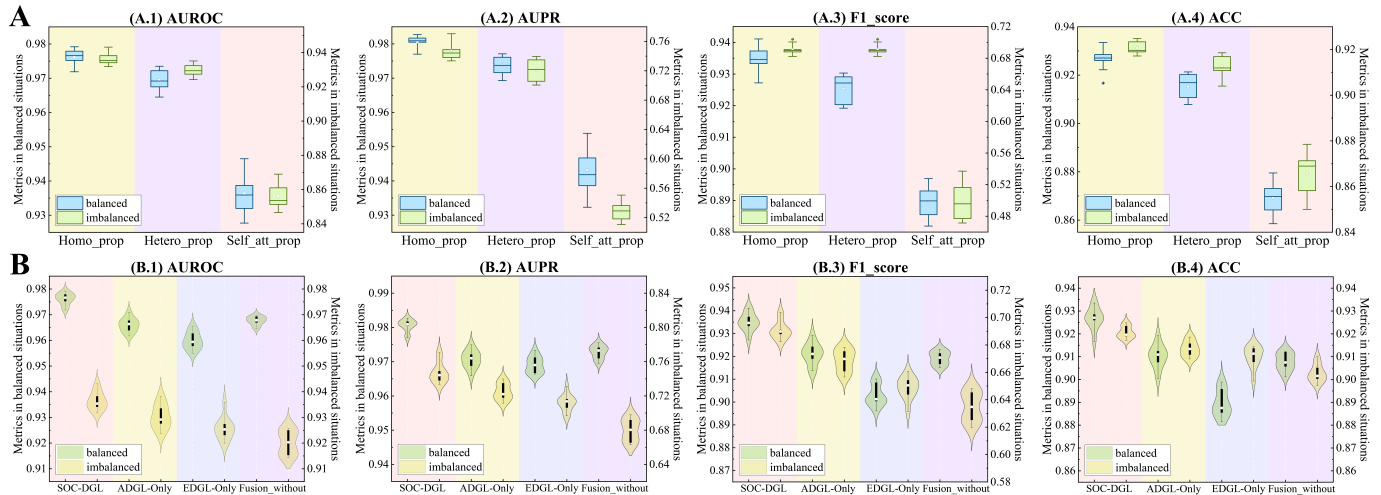


Fig. 4: Experimental validation conducted on the KIBA dataset. (A) Experimental evaluation of Homogeneous_prop, Heterogeneous_prop, and Self_attention_prop enhancement components in SOC-DGL for DTI prediction. (B) Ablation study of different components within the SOC-DGL model.

TABLE II: Warm start validation experiment on four benchmark imbalanced datasets using different loss functions.

Dataset	Loss	AUROC	AUPR	F1_score	ACC	Recall	Specificity	Precision
KIBA dataset	SLF	0.9329 ± 0.0042	0.7300 ± 0.0111	0.6758 ± 0.0090	0.9156 ± 0.0036	0.7054 ± 0.0265	0.9455 ± 0.0071	0.6501 ± 0.0230
	FLF	0.8983 ± 0.0078	0.6209 ± 0.0029	0.5400 ± 0.0023	0.8653 ± 0.0145	0.6530 ± 0.0175	0.8130 ± 0.0187	0.5411 ± 0.0016
	WLF	0.9309 ± 0.0035	0.7081 ± 0.0074	0.6675 ± 0.0056	0.9126 ± 0.0020	0.7032 ± 0.0263	0.9425 ± 0.0058	0.6363 ± 0.0164
	RLF	0.9364 ± 0.0036	0.7473 ± 0.0123	0.6908 ± 0.0068	0.9207 ± 0.0026	0.7103 ± 0.0182	0.9506 ± 0.0049	0.6730 ± 0.0177
Davis dataset	SLF	0.9171 ± 0.0046	0.7601 ± 0.0089	0.6907 ± 0.0144	0.9135 ± 0.0061	0.6618 ± 0.0234	0.9558 ± 0.0085	0.7233 ± 0.0334
	FLF	0.8983 ± 0.0106	0.6934 ± 0.0094	0.6132 ± 0.0122	0.8345 ± 0.0199	0.5938 ± 0.0443	0.8687 ± 0.0292	0.6376 ± 0.0161
	WLF	0.9158 ± 0.0031	0.7506 ± 0.0085	0.6790 ± 0.0038	0.9097 ± 0.0042	0.6516 ± 0.0221	0.9540 ± 0.0082	0.7102 ± 0.0592
	RLF	0.9192 ± 0.0045	0.7655 ± 0.0134	0.6918 ± 0.0129	0.9134 ± 0.0030	0.6642 ± 0.0338	0.9561 ± 0.0066	0.7238 ± 0.0230
BindingDB dataset	SLF	0.9684 ± 0.0064	0.8031 ± 0.0302	0.7553 ± 0.0350	0.9467 ± 0.0101	0.8162 ± 0.0311	0.9612 ± 0.0116	0.7060 ± 0.0036
	FLF	0.9067 ± 0.0151	0.7535 ± 0.0167	0.7807 ± 0.0151	0.8996 ± 0.0109	0.8139 ± 0.0140	0.9003 ± 0.0128	0.6994 ± 0.0268
	WLF	0.9578 ± 0.0074	0.7800 ± 0.0282	0.6899 ± 0.0405	0.9336 ± 0.0116	0.7326 ± 0.0392	0.9560 ± 0.0134	0.6564 ± 0.0685
	RLF	0.9790 ± 0.0034	0.8705 ± 0.0146	0.8057 ± 0.0177	0.9594 ± 0.0041	0.8406 ± 0.0246	0.9726 ± 0.0047	0.7744 ± 0.0304
DrugBank dataset	SLF	0.9150 ± 0.0094	0.7316 ± 0.0256	0.6998 ± 0.0205	0.9486 ± 0.0034	0.6158 ± 0.0267	0.9845 ± 0.0022	0.8104 ± 0.0206
	FLF	0.8206 ± 0.0096	0.4512 ± 0.0077	0.5127 ± 0.0133	0.8756 ± 0.0321	0.4733 ± 0.0331	0.9511 ± 0.0388	0.5755 ± 0.0414
	WLF	0.9208 ± 0.0073	0.7321 ± 0.0204	0.6795 ± 0.0164	0.9388 ± 0.0029	0.6696 ± 0.0242	0.8677 ± 0.0030	0.6897 ± 0.0249
	RLF	0.9295 ± 0.0076	0.7654 ± 0.0126	0.7211 ± 0.0104	0.9508 ± 0.0015	0.6567 ± 0.0210	0.9824 ± 0.0022	0.8004 ± 0.0174

datasets, demonstrating its effectiveness for imbalanced DTI prediction. Although RLF did not always yield the highest scores on individual metrics, it showed stable and robust performance. By incorporating a weighting parameter ϖ to reduce the weight of negative samples while maintaining the positive sample weight, RLF addressed class imbalance while preserving the model’s discriminative ability. These results, observed across four distinct imbalanced datasets, further validated RLF’s strong generalization capability.

G. Hyperparameter Tuning Experiments

To assess the model’s robustness across multiple benchmark datasets, this study focused on the hyperparameters within the ADGL and EDGL modules and performed “warm-start” experiments to systematically optimize these parameters.

1) *Optimization of ADGL Hyperparameters*: The number of convolutional layers (N) in the ADGL module was a critical hyperparameter influencing the model’s ability to capture the topological structure of drugs and targets. To assess the impact of different layer configurations on DTI prediction, experiments were conducted on both balanced and imbalanced versions of four benchmark datasets, with performance

evaluated across multiple metrics, as shown in Fig. 5 (A-D). The results indicated that a two-layer GCN consistently achieved the best performance, particularly on the BindingDB, DrugBank, and Davis datasets. For $N = 2$, the model excelled in AUROC, AUPR, and F1 score. However, on the KIBA dataset, $N = 1$ slightly outperformed $N = 2$ in AUROC (0.9838 vs. 0.9761) and AUPR (0.9872 vs. 0.9805), suggesting that a shallower GCN might have better captured global associations in this specific dataset. Overall, the two-layer setting expanded the receptive field, enhancing message passing and model expressiveness, while higher layer counts introduced complexity, increasing the risk of overfitting.

2) *Optimization of EDGL Hyperparameters*: This study focused on tuning key hyperparameters within the EDGL module. Specifically, this study investigated the total number of iterations (K) and the influence parameter (ω_α , denoted as α) using the KIBA dataset. To thoroughly assess the impact of these hyperparameters, this study experimented with a range of values for K and α , evaluating their effects on the performance of SOC-DGL. This study explored K values between 100 and 500 and adjusted α within the range of 0.05 to 0.25. The results presented in Fig. 5(E) showed that optimal performance

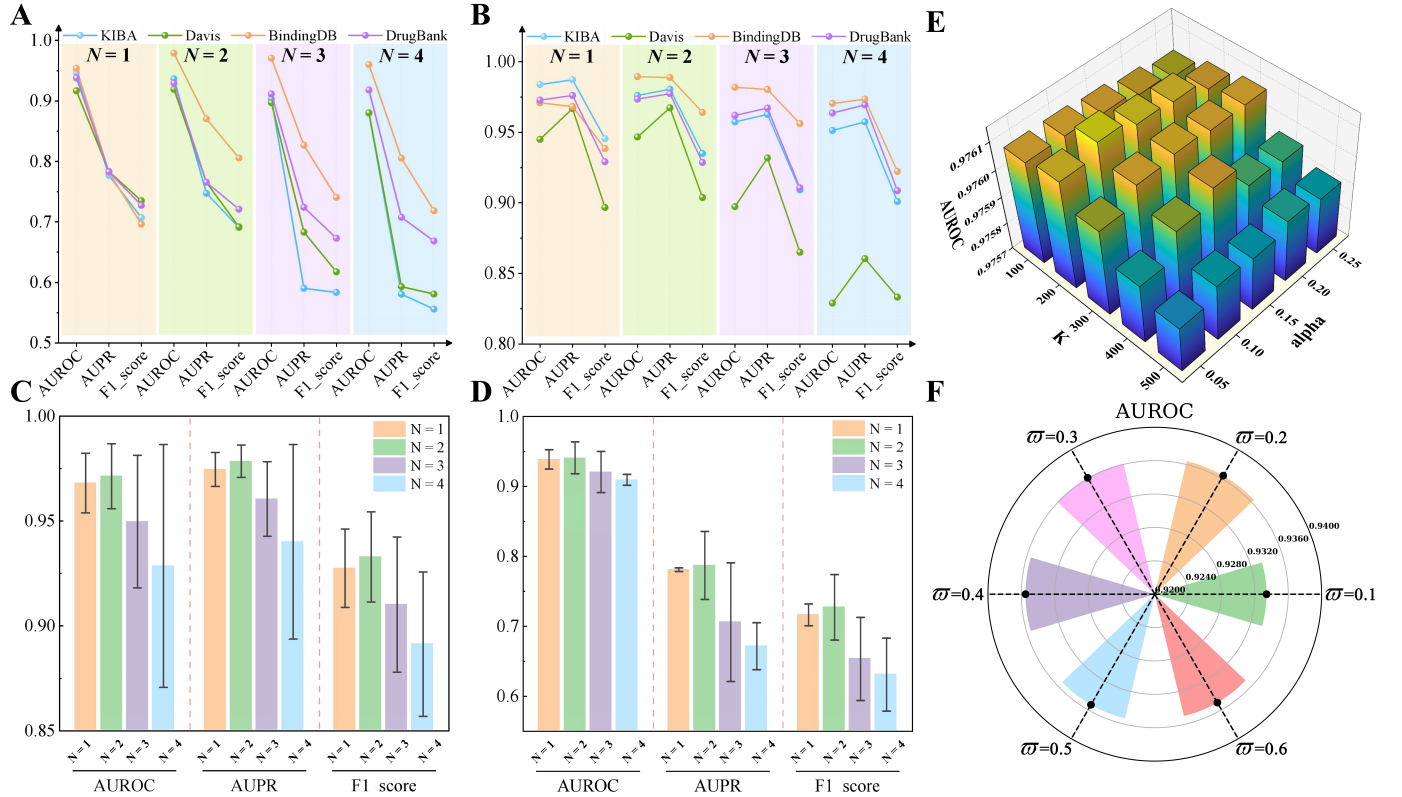


Fig. 5: SOC-DGL’s performance across AUROC, AUPR, and F1_score with different GCN layer settings on (A) four balanced datasets and (B) four imbalanced datasets. AUROC, AUPR, and F1_score of SOC-DGL under different GCN layer settings on (C) balanced datasets and (D) imbalanced datasets. (E) Hyperparameter tuning of K and α on the KIBA balanced dataset. (F) Hyperparameter tuning of ϖ on the KIBA imbalanced dataset.

was achieved when $K = 200$ and $\alpha = 0.20$, yielding an AUROC of 0.9761. This showed that a balanced and optimal choice of K and α improved performance, mitigating the negative impact of extreme values.

3) *Optimization of Adjustable Parameter ϖ* : Traditional imbalanced loss functions addressed the negative sample imbalance by adjusting the influence of positive samples based on the ratio of negative to positive samples. However, this approach did not provide an optimal solution for handling the imbalance between positive and negative samples. This seemingly reasonable correction may have resulted in an excessively large influence of positive sample loss on the total loss, leading to artificial positive sample imbalance. Therefore, an adjustable parameter was required to adjust the correction for positive samples, ensuring that the imbalance function effectively handled negative sample imbalance. This study investigated the effect of the adjustable parameter ϖ on imbalance processing through a hyperparameter experiment with $\varpi \in \{0.1, 0.2, 0.3, 0.4, 0.5, 0.6\}$. Results in Fig. 5 (F) showed that $\varpi = 0.2$ achieved the best performance, highlighting the necessity of introducing an adjustable parameter of appropriate size to adjust the correction for positive samples.

H. Drugs prediction for the key target ABL1 in Chronic Myeloid Leukemia

To assess the potential of SOC-DGL in discovering DTI in real-world applications, this study conducted a case study on

Chronic Myeloid Leukemia (CML), a myeloproliferative neoplasm with an incidence rate of approximately 1-2 cases per 100,000 adults, accounting for around 15% of newly diagnosed adult leukemia cases [38]. The primary pathogenesis of CML is driven by the fusion of the ABL1 gene on chromosome 9, a tyrosine kinase, with the Breakpoint Cluster Region (BCR) gene on chromosome 22, resulting in the formation of a malignant target that initiates and progresses the disease [39]. The ABL1 gene encodes a tyrosine kinase enzyme that activates downstream signaling pathways, regulating cell proliferation and differentiation [40]. CML onset is closely associated with ABL1 mutations, which lead to excessive cell proliferation, making it a key pathogenic factor in the disease [41].

In this case study, the edges associated with other drugs linked to ABL1 and applied SOC-DGL were removed to predict drugs targeting tyrosine protein kinase ABL1. The predicted DTI were ranked based on interaction scores, and the top 10 drugs were selected. Among these, 9 drugs were experimentally confirmed to target ABL1, as detailed in Tab. III, where ADGL-Edge represented the direct similarity edges learned through ADGL, and EDGL-Edge represented the higher-order similarity edges constructed by EDGL. Extensive friend and higher-order friend relationships, learned through ADGL and EDGL, were observed between these drugs, as shown in Fig. 6 (A). This demonstrated that ADGL and EDGL maintained strong biological interpretability when applied to real-world tasks. Two examples were provided to illustrate this. (1) For the third-ranked drug DB03878, ADGL learned

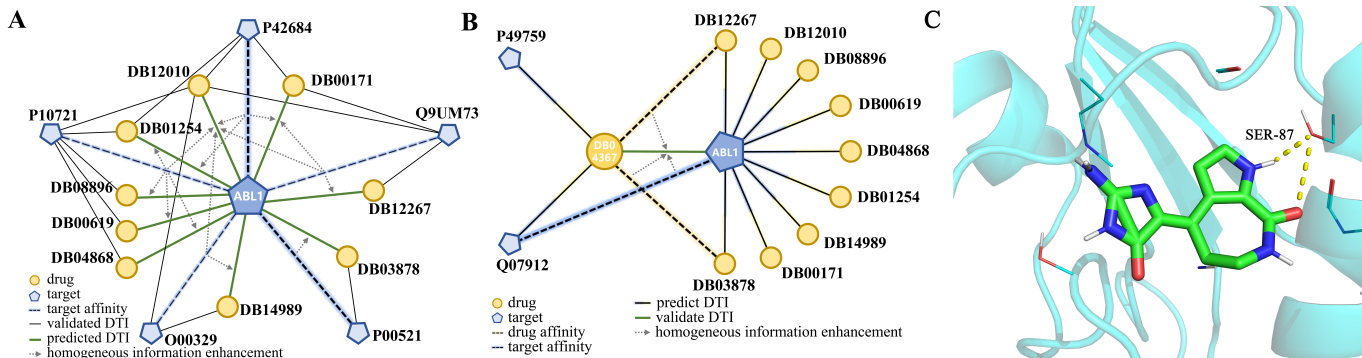


Fig. 6: Case study analysis. (A) SOC-DGL predicts the top 9 drugs targeting ABL1 and demonstrates the associations among them. (B) Verification of ADGL-Edge and EDGL-Edge between DeBromohymenialdisine and ABL1. (C) Perform a molecular docking experiment between DeBromohymenialdisine and ABL1. The yellow dashed lines represent hydrogen bonds.

TABLE III: SOC-DGL Prediction of the Top 10 Drugs Targeting Tyrosine-Protein Kinase ABL1.

No.	UniProtKB Entry	Name	Evidence	ADGL-Edge	EDGL-Edge
1	DB12010	Fostamatinib	Rolf et al. [32]	4	6
2	DB00171	ATP	Inming et al. [33]	2	1
3	DB03878	N-[4-Methyl-3-[4-(3-Pyridinyl)-2-Pyrimidinyl]Amino]Phenyl]-3-Pyridinecarboxamide	Berman et al. [34]	1	0
4	DB08896	Regorafenib	DrugBank	1	0
5	DB12267	Brigatinib	Markham [35]	1	0
6	DB14989	Umbralisib	DrugBank	1	0
7	DB00619	Imatinib	Haberler et al. [36]	1	0
8	DB01254	Dasatinib	Piccaluga et al. [37]	2	1
9	DB04868	Nilotinib	DrugBank	1	0
10	DB04367	DeBromohymenialdisine	None	3	1

high similarity information between ABL1 and P00521 via extensive friendship and high heterogeneity between P00521 and DB03878, predicting a potential association between DB03878 and ABL1. (2) For the top-ranked drug DB12010, SOC-DGL first learned four direct similarity relationships between ABL1 and P10721, P42684, Q9UM73, and O00329 through the ADGL module. Then, using EDGL, higher-order friendships were established, with DB12010 acting as an intermediary to create six (C_4^2) indirect friend channels, indirectly enhancing the higher-order similarity information between P10721, P42684, Q9UM73, and O00329, thus learning a potential association between ABL1 and DB01254.

Notably, SOC-DGL predicted DeBromohymenialdisine as the 10th-ranked drug, which is a cyclin-dependent kinase inhibitor with pharmacological activity in the treatment of osteoarthritis and Alzheimer’s disease [42]. Upon searching databases and relevant literature, this study found that the direct association between DeBromohymenialdisine and ABL1 had not been confirmed by any database or publication. However, SOC-DGL’s prediction suggested a potential link between the two. As shown in Fig. 6 (B) and Tab. III, further investigation revealed that SOC-DGL first learned three direct similarity relations between DB04367, DB12267, and DB03878 through the ADGL module, as well as an interaction between DB04367 and Q07912. Subsequently, through the EDGL module, a friendship pathway was constructed using ABL1 as an intermediary, indirectly enhancing the higher-order similarity information between DB12267 and DB03878, and thereby uncovering a potential connection between ABL1 and DB04367. To further verify the binding

degree of DB04367 and ABL1 at the molecular level, we conducted molecular docking experiments on them with Pymol and AutoDockTools, shown in Fig. 6 (C). The docking results indicated that DB04367 formed intermolecular forces with the amino acid residues in ABL1, further confirming the interaction between DB04367 and ABL1. These findings highlighted the remarkable ability of SOC-DGL to identify potential DTI through two distinct drug-target friendship strategies and validated the predictions of SOC-DGL, demonstrating its reliability in recognizing potential DTI and providing valuable insights for biological research.

V. CONCLUSION

In this study, SOC-DGL, a novel graph learning framework was proposed for DTI prediction. Drawing inspiration from real-world social interactions, this paper designed ADGL, which captures the direct global association and similarity information between drugs and targets based on extensive social connections. Additionally, EDGL leverages an even-polynomial graph filter driven by balance theory to extract higher-order similarity information from the heterogeneous drug-target graph, akin to high-order social interactions. This dual approach enhances prediction accuracy and demonstrates robust performance under data imbalance conditions. Experimental results on four benchmark datasets demonstrate that SOC-DGL outperforms existing state-of-the-art methods in both balanced and imbalanced data settings. The success of SOC-DGL in potential DTI (between DB01254 and ABL1) prediction highlights the importance of leveraging homogeneous information aggregation in capturing complex indirect

relationships within biological networks. Although SOC-DGL performs well in DTI prediction, its performance still limited by data quality, and future work could involve incorporating more biological knowledge or employing advanced data augmentation techniques to reduce noise and bias in datasets.

VI. APPENDIX

A. Datasets

To comprehensively evaluate the performance and applicability of the proposed method, we select four representative benchmark datasets: the KIBA dataset, the Davis dataset, the BindingDB dataset, and the DrugBank dataset.

1) *KIBA dataset*: In the KIBA dataset, some drugs and proteins do not have direct affinity metrics. However, it still contains comprehensive bioactivity measurement data between 2,111 kinase inhibitors and 229 kinases, including but not limited to key parameters such as $K(d)$, $K(i)$, and IC50. Notably, DTI are considered to have binding affinity when the $K(d)$ value is below 30 units. To further optimize and utilize this dataset, we employ the Therapeutics Data Commons (TDC), a drug discovery application tool developed by Huang et al. [43] in 2022. Through the download and filtering capabilities of the TDC tool, we successfully obtain a refined dataset covering 1,720 drugs and 220 targets. This binary processed DTI dataset comprises 22,154 DTI, providing rich information and a solid foundation for our research and model training.

2) *Davis dataset*: The Davis dataset is a highly valuable resource in the field of DTI research, meticulously documenting the $K(d)$ values obtained from wet laboratory tests between 72 kinase inhibitors and 442 kinases. This dataset covers over 80% of the human catalytic protein kinase family, providing a wealth of information for understanding the bioactivity of kinase inhibitors. To further enhance the practicality of the data and the accuracy of analysis, we employ the Therapeutics Data Commons tool to process the Davis dataset. Through TDC's advanced filtering and analysis capabilities, we successfully refine 7,320 positive samples, which encompass 68 drugs and 379 targets. This binary processed DTI dataset offers a more precise and comprehensive collection of positive samples for bioinformatics research, improving the quality of the data.

3) *BindingDB dataset*: BindingDB is a public dataset specifically designed to store experimentally measured binding affinities between small molecules (ligands) and their corresponding target biomolecules (targets). With an extensive dataset encompassing $K(d)$ values for 10,665 drugs and 1,413 targets, BindingDB provides researchers with a valuable platform for gaining insights into DTI. To further optimize this data for specific research needs and enhance its usability, we employ the TDC tool and retain 9,166 DTI between 3,400 drugs and 886 targets.

4) *DrugBank dataset*: In ensuring the accuracy and reliability of the dataset, we implement a series of stringent quality control measures. Specifically, we conduct a thorough review of the drug molecules in the dataset, manually filtering out those drug sequences that cannot be effectively recognized through the Simplified Molecular Input Line-Entry System (SMILES) format using RDKit [44]. To address the sparsity

issue of the DTI dataset, we further optimize the dataset by retaining only those drugs that interact with at least two targets. After these carefully designed selection processes, we ultimately obtain a dataset comprising 6,871 verified DTI, covering 1,821 drugs and 1,447 targets.

5) *Preprocessing of datasets*: For each benchmark dataset, we extract various features of drugs and targets based on the SMILES sequences of drugs and the UniProt IDs of targets. For drug sequences, we use the RDKit software package to extract Molecular Access System (MACCS) keys fingerprints [45], topological (TOP) fingerprints [46], and Morgan fingerprints [47], which represent three distinct aspects of the molecular features. For target sequences, to provide a more systematic description of target sequences and their physicochemical properties, we employ the iLearn software package to calculate amino acid composition (AAC), Moran autocorrelation (MORAN) [48], Composition/Transition/Distribution (CTD) [49], and pseudo-amino acid composition (PAAC) [50], which encompass four different aspects of target features.

In drug discovery and bioinformatics, selecting negative samples is crucial. Positive samples are drugs known to interact with targets, while negative samples are those with unknown interactions. To improve model performance, we employ an association-based negative sampling method that selects more reliable negative samples by leveraging drug similarity. If a drug's neighbors (high-similarity drugs) interact with a target, it is likely to do so as well. Conversely, drugs with low similarity to known positives are less likely to share common targets and can be considered negative samples, reducing the model's bias toward positive interactions.

B. Detailed Process of Multi-view Learning

Taking the application of multi-view learning in drug affinity matrices as an example, the specific process of multi-view learning can be detailed as follows. First, we respectively represent the MACC feature matrix, the Morgan feature matrix and the TOP feature matrix as $Y_1 \in \mathbb{R}^{v_1 \times n}$, $Y_2 \in \mathbb{R}^{v_2 \times n}$, and $Y_3 \in \mathbb{R}^{v_3 \times n}$, where v_1 represents the dimensionality of the MACC drug features, v_2 represents the dimensionality of the Morgan drug features, v_3 represents the dimensionality of the TOP drug features, and n represents the number of drugs. Consequently, the combined drug feature matrix Y can be obtained, expressed as follows:

$$Y = \begin{bmatrix} Y_1^T \\ Y_2^T \\ Y_3^T \end{bmatrix} \in \mathbb{R}^{(v_1+v_2+v_3) \times n} \quad (15)$$

Then, we define $v = v_1 + v_2 + v_3$ to represent the total number of perspectives. Following this, we introduce four auxiliary matrices A , $C1$, $C2$, and $C3$, each of which is a three-dimensional matrix of size $v \times n_d \times n_d$. These four auxiliary matrices encompass v perspectives (distinct feature sets within multi-view learning), with each perspective having matrices of identical row and column dimensions. Specifically, A denotes the relationship matrix among the various views, $C1$ is the auxiliary matrix for different views after singular value

thresholding, $C2$ is the auxiliary matrix for different views following sparsity processing, and $C3$ is the auxiliary matrix that integrates information from multiple views. These auxiliary matrices are initialized to zero. Concurrently, we incorporate four Lagrange multiplier matrices $\lambda 1 \in \mathbb{R}^{(v+1)n_d \times n_d}$, $\lambda 2 \in \mathbb{R}^{v \times n_d \times n_d}$, $\lambda 3 \in \mathbb{R}^{v \times n_d \times n_d}$, and $\lambda 4 \in \mathbb{R}^{v \times n_d \times n_d}$, and set five hyperparameters μ , β_1 , β_2 , λ , and μ_{\max} , with only the parameter μ being continuously updated. For all formulas in this section, the subscript i signifies the index of a particular view, where $i = 0, 1, \dots, v$. We define C_{sum} , which represents the sum of the values of the $C2$ matrices of all views except view i itself.

$$C_{\text{sum}_i} = \sum_{i' \neq i} C2_{i'} \quad (16)$$

Then, we update the auxiliary matrix A iteratively. It updates the main relationship matrix A of each view by integrating the auxiliary matrices of all views and the Lagrange multiplier matrices. The formula is as follows:

$$A_i = \mu_i(K + 3I)^{-1} \cdot \left(\mu_i(K + C1 + C2 + C3) - (\lambda 2 + \lambda 3 + \lambda 4) + Y_i^T \lambda 1 \right) \quad (17)$$

where $K = Y_i^T Y_i$, and I is the identity matrix. Subsequently, we update the auxiliary matrix $C1$ iteratively and perform singular value thresholding on it. This process can effectively reduce the dimensionality and denoise the matrix. We perform singular value decomposition:

$$A_i + \frac{\lambda 3}{\mu_i} = U_i \Sigma_i V_i^T \quad (18)$$

where U_i and V_i are orthogonal matrices, and Σ_i is the diagonal matrix containing the singular values. Then, the singular value matrix Σ_i is thresholded to obtain $\Sigma'_i = \max(\Sigma_i - \frac{\beta_1}{\mu_i}, 0)$. Using the thresholded singular value matrix to reconstruct the matrix $C1$, we get $C1_i = U_i \Sigma'_i V_i^T$, and this completes the iterative update for $C1$. Next, we update $C2$ through soft thresholding, with the formula as follows:

$$C2 = \max\left(A + \frac{\lambda 2}{\mu_i} - \frac{\beta_2}{\mu_i}, 0\right) + \min\left(A + \frac{\lambda 2}{\mu_i} + \frac{\beta_2}{\mu_i}, 0\right) \quad (19)$$

This operation updates the auxiliary matrix $C2$ for each view, effectively making the matrix sparser. Then, by integrating information from other matrices, we update the current matrix $C3$ to promote consistency and convergence, with the formula as follows:

$$C3_i = \frac{2\lambda(v-1)C_{\text{sum}_i} + \mu_i A_i + \lambda 4_i}{2\lambda(v-1) + \mu_i} \quad (20)$$

Subsequently, we adjust the Lagrange multipliers incrementally through the differences in constraint conditions, ensuring that the final solution satisfies all constraint conditions. The formula for this is as follows:

$$\begin{cases} \lambda 1 = \lambda 1 + \mu_i(Y_i - X_i A_i) \\ \lambda 2 = \lambda 2 + \mu_i(A_i - C2_i) \\ \lambda 3 = \lambda 3 + \mu_i(A_i - C1_i) \\ \lambda 4 = \lambda 4 + \mu_i(A_i - C3_i) \end{cases} \quad (21)$$

In the iterative optimization algorithm, convergence checking is an important step to determine whether the algorithm has achieved the expected precision, thus allowing the iteration to be terminated. Specifically, the goal of convergence checking is to ensure that the differences (errors) between various matrices are within an allowable error threshold. In the model, convergence checking is implemented by calculating the error values between different matrices, with the formulas as follows:

$$\begin{cases} err_1 = \max |A_i - C1_i| \\ err_2 = \max |A_i - C2_i| \\ err_3 = \max |A_i - C3_i| \\ err_4 = \max |A_{i-1} - A_i| \end{cases} \quad (22)$$

If all errors are less than the threshold value $\varepsilon = 0.000001$, the algorithm is considered to have converged. It should be noted that during one iteration, i starts from zero and gradually increases to the number of views v , with matrix updates performed at each step. That is, in one iteration, the matrices mentioned earlier are all updated v times. When one iteration ends, i is reset to zero and the process of incrementing and updating matrices begins again. The iteration stops after 100 iterations or if the algorithm does not converge. As previously mentioned, μ is also updated with each iteration. In the iterative optimization algorithm, updating μ serves to control the weight of different terms in the objective function, allowing for a gradual approach to the optimal solution with each iteration. Specifically, μ is a regularization parameter that is updated according to certain rules in each iteration. We set a maximum value μ_{\max} , and an increment factor ρ to update the value of μ :

$$\mu_{t+1} = \min(\rho \mu_t, \mu_{\max}) \quad (23)$$

where ρ is a constant greater than 1, and μ_{\max} is the upper limit of μ . Once all iterations are completed, we obtain the final auxiliary matrix $C2$ after the iterative updates. We then define a matrix C_{avg} , which represents the average of the $C2$ matrices from all views:

$$C_{\text{avg}} = \frac{1}{v} \sum_j C2_j \quad (24)$$

Ultimately, through pairwise multi-view learning on multiple drug features, we derive the drug affinity matrix $A_{DD} = |C_{\text{avg}}| + |C_{\text{avg}}^T|$. Similarly, we can obtain A_{TT} using the aforementioned method. It is important to note that we use the iLearn software package to calculate features for the target sequences in these four different aspects (ACC, MORAN, CDT, PAAC), hence the number of views at this time is $v = v_1 + v_2 + v_3 + v_4$. Subsequently, we apply the min-max normalization method to both A_{DD} and A_{TT} .

C. Comparison with Baseline Methods in "warm-start" experiments

To validate the effectiveness and superiority of SOC-DGL, we conducted comparative experiments with four leading methods that were widely recognized in DTI prediction. These models included GraphDTA [27], LRSpNM [28], MLMC [29], MULGA [30], and MMDG-DTI [31]. The detailed results of

TABLE IV: Performance comparison of SOC-DGL with baseline methods on four datasets.

Dataset	Situation	Model	Year	AUROC	AUPR	F1_score	ACC	Recall	Specificity	Precision	
KIBA	balanced	GraphDTA	2021	0.9295	0.9355	0.8783	0.8566	0.9237	0.7710	0.8372	
		LRSpNM	2021	0.9224	0.9382	0.8740	0.8740	0.8740	0.7730	0.8371	
		MLMC	2022	0.9484	0.9592	0.9049	0.8935	0.9038	0.8803	0.9059	
		MULGA	2023	0.9479	0.9551	0.8984	0.8773	0.9404	0.7911	0.8600	
		MMDG-DTI	2025	0.9586	0.9646	0.9083	0.8949	0.9318	0.8483	0.8858	
		SOC-DGL	\	0.9761	0.9805	0.9350	0.9268	0.9373	0.9133	0.9328	
	imbalanced	GraphDTA	2021	0.9195	0.6500	0.6121	0.8911	0.6895	0.9198	0.5502	
		LRSpNM	2021	0.9132	0.6904	0.6339	0.8998	0.6900	0.9299	0.5863	
		MLMC	2022	0.9329	0.7462	0.6874	0.9192	0.7084	0.9494	0.6675	
		MULGA	2023	0.8918	0.5556	0.5628	0.8666	0.6808	0.8934	0.4796	
		MMDG-DTI	2025	0.9245	0.7193	0.6639	0.9102	0.6998	0.9391	0.6273	
		SOC-DGL	\	0.9364	0.7473	0.6908	0.9207	0.7103	0.9506	0.6730	
	Davis	balanced	GraphDTA	2021	0.9015	0.9324	0.8707	0.8330	0.9016	0.7195	0.8418
			LRSpNM	2021	0.8930	0.9256	0.8644	0.8255	0.9083	0.6951	0.8250
MLMC			2022	0.9072	0.9395	0.8712	0.8712	0.9098	0.7177	0.8356	
MULGA			2023	0.9158	0.9451	0.8790	0.8561	0.8539	0.8596	0.9058	
MMDG-DTI			2025	0.9356	0.9647	0.8905	0.8627	0.9057	0.7934	0.8758	
SOC-DGL			\	0.9467	0.9673	0.9038	0.8816	0.9097	0.8372	0.8985	
imbalanced		GraphDTA	2021	0.8486	0.6024	0.5514	0.8797	0.5096	0.9425	0.6006	
		LRSpNM	2021	0.9108	0.7067	0.6415	0.8961	0.6348	0.9409	0.6517	
		MLMC	2022	0.9110	0.7253	0.6704	0.9057	0.6530	0.9492	0.6888	
		MULGA	2023	0.8812	0.6179	0.5710	0.8698	0.5874	0.9187	0.5556	
		MMDG-DTI	2025	0.9087	0.7787	0.7369	0.9326	0.6503	0.9805	0.8409	
		SOC-DGL	\	0.9192	0.7655	0.6918	0.9134	0.6642	0.9561	0.7238	
BindingDB		balanced	GraphDTA	2021	0.9325	0.9271	0.8719	0.8605	0.9103	0.8063	0.8366
			LRSpNM	2021	0.8514	0.5771	0.5533	0.8706	0.5464	0.9263	0.5602
	MLMC		2022	0.8797	0.9285	0.8707	0.8750	0.8237	0.9286	0.9233	
	MULGA		2023	0.9874	0.9859	0.9678	0.9660	0.9818	0.9490	0.9542	
	MMDG-DTI		2025	0.9620	0.9661	0.9181	0.9172	0.9172	0.9340	0.9340	
	SOC-DGL		\	0.9894	0.9888	0.9641	0.9627	0.9677	0.9574	0.9606	
	imbalanced	GraphDTA	2021	0.9718	0.8099	0.7614	0.9320	0.7724	0.9718	0.7508	
		LRSpNM	2021	0.8481	0.5727	0.5866	0.9096	0.6383	0.9399	0.5426	
		MLMC	2022	0.8992	0.8260	0.7990	0.9617	0.7584	0.9844	0.8443	
		MULGA	2023	0.9706	0.8366	0.7188	0.9444	0.6991	0.9721	0.7395	
		MMDG-DTI	2025	0.9149	0.7428	0.6967	0.8980	0.6504	0.9508	0.7429	
		SOC-DGL	\	0.9790	0.8705	0.8057	0.9594	0.8406	0.9726	0.7744	
	DrugBank	balanced	GraphDTA	2021	0.8762	0.8676	0.8304	0.8033	0.9242	0.6719	0.7539
			LRSpNM	2021	0.7563	0.8206	0.7016	0.6687	0.7522	0.5790	0.6573
MLMC			2022	0.8637	0.9126	0.8371	0.8415	0.7828	0.9052	0.8995	
MULGA			2023	0.9715	0.9743	0.9165	0.9141	0.9112	0.9171	0.9219	
MMDG-DTI			2025	0.9626	0.9658	0.9180	0.9159	0.9083	0.9240	0.9281	
SOC-DGL			\	0.9735	0.9774	0.9286	0.9267	0.9208	0.9331	0.9369	
imbalanced		GraphDTA	2021	0.8450	0.4268	0.4564	0.8764	0.5336	0.9133	0.3987	
		LRSpNM	2021	0.7752	0.5480	0.5437	0.9257	0.4577	0.9758	0.6695	
		MLMC	2022	0.8594	0.7330	0.7043	0.9498	0.6181	0.9853	0.8185	
		MULGA	2023	0.9259	0.7179	0.6667	0.9358	0.6579	0.9659	0.6756	
		MMDG-DTI	2025	0.9051	0.6978	0.6717	0.9381	0.6522	0.9688	0.6943	
		SOC-DGL	\	0.9295	0.7654	0.7211	0.9508	0.6567	0.9824	0.8004	

the comparative experiments on these baseline datasets were presented in Appendix Tab. IV.

1) *GraphDTA*: GraphDTA, proposed by Thin Nguyen et al. in 2021, is a graph neural network-based model for predicting drug-target binding affinity. It represents drug molecules as graphs, using graph convolution to capture their spatial and chemical properties, improving DTI prediction accuracy by integrating various drug and target features.

2) *LRSpNM*: LRSpNM, introduced by Gaoyan Wu et al. in 2021, predicts drug-target interactions using similarity information and dynamic pre-filling of unknown interactions. It employs low-rank matrix approximation, loss functions, and Laplacian regularization, utilizing the ADMM algorithm for efficient computation on large bioinformatics datasets.

3) *MLMC*: MLMC, proposed by Yixin Yan et al. in 2022, predicts drug-disease associations by integrating multi-view learning for similarity information and matrix completion to

fill missing values in the association matrix, improving the model’s predictive power for unknown drug-disease pairs.

4) *MULGA*: MULGA, proposed by Jiani Ma et al. in 2023, is a multi-view graph autoencoder framework for DTI and drug repurposing prediction. It learns affinity matrices and infers missing interactions using a novel “guilt-by-association” negative sampling method, improving predictive accuracy.

5) *MMDG-DTI*: MMDG-DTI, proposed by Yang Hua et al. in 2025, addresses domain-specific biases in existing models by using pre-trained LLMs to extract generalized features and a hybrid GNN for structural learning. It enhances generalization through Domain Adversarial Training, contrastive learning, and multi-modal feature fusion.

D. Analysis of the even-polynomial graph filter in EDGL

Higher-order homogeneous information enhancement by the even-polynomial graph filter was primarily designed to

capture direct relationships between adjacent nodes. In the context of a drug-target network, this approach emphasized identifying the direct interactions between drugs and targets. It effectively highlighted the interactions between first-order neighbors, which were nodes directly connected by an edge. Higher-order homogeneous information enhancement by the even-polynomial graph filter retained odd-order monomials while discarding even-order terms, as formulated below:

$$Y' = f(\hat{X}, P) = \sum_{k=0}^{\lfloor \frac{K}{2} \rfloor} \alpha_k P^{2k-1} \hat{X} \quad (25)$$

Regarding the self-attention mechanism, its application in graph neural networks captured the complex interactions between nodes in a graph. By calculating attention weights, the self-attention mechanism assigned different weights to different neighboring nodes, thereby selectively aggregating important neighboring information. It focused on the most critical relationships for the prediction task, whether direct or indirect. For the self-attention mechanism, we used the result H' obtained from ADGL as the input and performed three different linear transformations on the input vector to obtain Q (Query), K (Key), and V (Value), where $Q = H'W^Q$, $K = H'W^K$, $V = H'W^V$. Here, $W^Q, W^K, W^V \in \mathbb{R}^{d \times d_k}$ were trainable weight matrices, and here $d_k = m$. Then, the formula for self-attention was obtained as:

$$Y'' = \text{softmax}\left(\frac{QK^T}{\sqrt{m}}\right) \cdot V \quad (26)$$

E. Validation experiment on imbalanced loss function in imbalanced datasets

The standard binary cross-entropy loss function was a commonly used loss function suitable for balanced datasets, but it might have caused the model to favor the majority class in imbalanced datasets. The focal loss [51] aimed to address class imbalance by reducing the weight of easily classified samples while increasing the weight of hard-to-classify samples. The weighted binary cross-entropy loss function balanced the disparity between positive and negative samples by assigning higher weights to the minority class. The reduced negative weighted binary cross-entropy loss function reduced the weight of negative samples while keeping the weight of positive samples unchanged, mitigating the impact of imbalanced data on model performance. The formulas for the four loss functions were as follows:

$$\mathcal{L}_S = -\frac{1}{n_d \cdot n_t} \left(\sum_{(i,j) \in y^+} \log(h_{ij}^*) + \sum_{(i,j) \in y^-} \log(1 - h_{ij}^*) \right) \quad (27)$$

$$\mathcal{L}_F = -\frac{|y^-|}{|y^+|} (1 - h_{ij}^*)^\gamma \log(h_{ij}^*) \quad (28)$$

$$\mathcal{L}_W = -\frac{1}{n_d \cdot n_t} \left(\frac{|y^-|}{|y^+|} \sum_{(i,j) \in y^+} \log(h_{ij}^*) + \sum_{(i,j) \in y^-} \log(1 - h_{ij}^*) \right) \quad (29)$$

$$\mathcal{L}_R = -\frac{1}{n_d \cdot n_t} \left(\varpi \frac{|y^-|}{|y^+|} \sum_{(i,j) \in y^+} \log(h_{ij}^*) + \sum_{(i,j) \in y^-} \log(1 - h_{ij}^*) \right) \quad (30)$$

where \mathcal{L}_S , \mathcal{L}_F , \mathcal{L}_W , and \mathcal{L}_R were Standard Binary Cross-Entropy Loss (SLF), Focal Loss with Dynamic Scaling (FLF), Weighted Binary Cross-Entropy Loss (WLF), and Weighted Binary Cross-Entropy Loss with Reduced Negative Samples (RLF), respectively. n_d was the number of drugs in the dataset, n_t was the number of targets in the dataset, $|y^+|$ represented the number of positive samples, and $|y^-|$ represented the number of negative samples. h_{ij}^* represented the model's predicted probability of interaction between drug i and target j . γ was an adjustment parameter used to reduce the weight of easily classified samples and increase the weight of hard-to-classify samples. ϖ was also an adjustment parameter, used to reduce the weight of negative samples while keeping the weight of positive samples unchanged.

REFERENCES

- [1] J.-P. Jourdan, R. Bureau, C. Rochais, and P. Dallemagne, "Drug repositioning: a brief overview," *Journal of Pharmacy and Pharmacology*, vol. 72, no. 9, pp. 1145–1151, 2020.
- [2] C. R. Chong and D. J. Sullivan Jr, "New uses for old drugs," *Nature*, vol. 448, no. 7154, pp. 645–646, 2007.
- [3] M. A. Farha and E. D. Brown, "Drug repurposing for antimicrobial discovery," *Nature microbiology*, vol. 4, no. 4, pp. 565–577, 2019.
- [4] M. Wang, X. Lei, L. Liu, J. Chen, and F.-X. Wu, "Giae-dti: Predicting drug-target interactions based on heterogeneous network and gin-based graph autoencoder," *IEEE Journal of Biomedical and Health Informatics*, 2024.
- [5] Q. Zhao, H. Zhao, K. Zheng, and J. Wang, "Hyperattentiondti: improving drug-protein interaction prediction by sequence-based deep learning with attention mechanism," *Bioinformatics*, vol. 38, no. 3, pp. 655–662, 2022.
- [6] W. Zhao, Y. Yu, G. Liu, Y. Liang, D. Xu, X. Feng, and R. Guan, "Msi-dti: predicting drug-target interaction based on multi-source information and multi-head self-attention," *Briefings in Bioinformatics*, vol. 25, no. 3, p. bbae238, 2024.
- [7] W. Shi, H. Yang, L. Xie, X.-X. Yin, and Y. Zhang, "A review of machine learning-based methods for predicting drug-target interactions," *Health Information Science and Systems*, vol. 12, no. 1, p. 30, 2024.
- [8] T. Zhao, Y. Hu, L. R. Valsdottir, T. Zang, and J. Peng, "Identifying drug-target interactions based on graph convolutional network and deep neural network," *Briefings in Bioinformatics*, vol. 22, no. 2, pp. 2141–2150, 2021.
- [9] M. Yang, G. Wu, Q. Zhao, Y. Li, and J. Wang, "Computational drug repositioning based on multi-similarities bilinear matrix factorization," *Briefings in Bioinformatics*, vol. 22, no. 4, p. bbae267, 2021.
- [10] Y. Shang, X. Ye, Y. Futamura, L. Yu, and T. Sakurai, "Multiview network embedding for drug-target interactions prediction by consistent and complementary information preserving," *Briefings in Bioinformatics*, vol. 23, no. 3, p. bbac059, 2022.
- [11] E. Zixuan, G. Qiao, G. Wang, and Y. Li, "Gsl-dti: Graph structure learning network for drug-target interaction prediction," *Methods*, vol. 223, pp. 136–145, 2024.
- [12] M. A. Thafar, R. S. Olayan, H. Ashoor, S. Albaradei, V. B. Bajic, X. Gao, T. Gjobori, and M. Essack, "Dtigems+: drug-target interaction prediction using graph embedding, graph mining, and similarity-based techniques," *Journal of Cheminformatics*, vol. 12, pp. 1–17, 2020.
- [13] Y. Sun, Y. Y. Li, C. K. Leung, and P. Hu, "ingnn-dti: prediction of drug-target interaction with interpretable nested graph neural network and pretrained molecule models," *Bioinformatics*, vol. 40, no. 3, p. btae135, 2024.
- [14] Y. Xie, X. Wang, P. Wang, and X. Bi, "A pseudo-label supervised graph fusion attention network for drug-target interaction prediction," *Expert Systems with Applications*, vol. 259, p. 125264, 2025.
- [15] K. Shao, Y. Zhang, Y. Wen, Z. Zhang, S. He, and X. Bo, "Dti-heta: prediction of drug-target interactions based on gcnn and gat on heterogeneous graph," *Briefings in Bioinformatics*, vol. 23, no. 3, p. bbac109, 2022.

- [16] M. Wang, X. Lei, L. Liu, J. Chen, and F.-X. Wu, "Giae-dti: Predicting drug-target interactions based on heterogeneous network and gin-based graph autoencoder," *IEEE Journal of Biomedical and Health Informatics*, pp. 1–14, 2024.
- [17] M. Wang, X. Lei, L. Guo, M. Chen, and Y. Pan, "Dhgt-dti: Advancing drug-target interaction prediction through a dual-view heterogeneous network with graphsage and graph transformer," *Journal of Pharmaceutical Analysis*, p. 101336, 2025.
- [18] Y. Mi, H. Chen, C. Luo, S.-J. Horng, and T. Li, "Unsupervised feature selection with high-order similarity learning," *Knowledge-Based Systems*, vol. 285, p. 111317, 2024.
- [19] H. Wang, Y. Ji, P. Song, and Z. Liu, "High-order similarity learning based domain adaptation for speech emotion recognition," *Applied Acoustics*, vol. 231, p. 110555, 2025.
- [20] H. Peng, H. Wang, Y. Hu, W. Zhou, and H. Cai, "Multi-dimensional clustering through fusion of high-order similarities," *Pattern Recognition*, vol. 121, p. 108108, 2022.
- [21] D. Cartwright and F. Harary, "Structural balance: a generalization of heider's theory," *Psychological review*, vol. 63, no. 5, p. 277, 1956.
- [22] J. Tang, A. Szwajda, S. Shakyawar, T. Xu, P. Hintsanen, K. Wennerberg, and T. Aittokallio, "Making sense of large-scale kinase inhibitor bioactivity data sets: a comparative and integrative analysis," *Journal of Chemical Information and Modeling*, vol. 54, no. 3, pp. 735–743, 2014.
- [23] M. I. Davis, J. P. Hunt, S. Herrgard, P. Ciceri, L. M. Wodicka, G. Pallares, M. Hocker, D. K. Treiber, and P. P. Zarrinkar, "Comprehensive analysis of kinase inhibitor selectivity," *Nature biotechnology*, vol. 29, no. 11, pp. 1046–1051, 2011.
- [24] T. Liu, Y. Lin, X. Wen, R. N. Jorissen, and M. K. Gilson, "Bindingdb: a web-accessible database of experimentally determined protein–ligand binding affinities," *Nucleic acids research*, vol. 35, no. suppl.1, pp. D198–D201, 2007.
- [25] D. S. Wishart, Y. D. Feunang, A. C. Guo, E. J. Lo, A. Marcu, J. R. Grant, T. Sajed, D. Johnson, C. Li, Z. Sayeeda *et al.*, "Drugbank 5.0: a major update to the drugbank database for 2018," *Nucleic acids research*, vol. 46, no. D1, pp. D1074–D1082, 2018.
- [26] H. Ding, I. Takigawa, H. Mamitsuka, and S. Zhu, "Similarity-based machine learning methods for predicting drug–target interactions: a brief review," *Briefings in bioinformatics*, vol. 15, no. 5, pp. 734–747, 2014.
- [27] T. Nguyen, H. Le, T. P. Quinn, T. Nguyen, T. D. Le, and S. Venkatesh, "Graphdta: predicting drug–target binding affinity with graph neural networks," *Bioinformatics*, vol. 37, no. 8, pp. 1140–1147, 2021.
- [28] G. Wu, M. Yang, Y. Li, and J. Wang, "De novo prediction of drug–target interactions using laplacian regularized Schatten p-norm minimization," *Journal of Computational Biology*, vol. 28, no. 7, pp. 660–673, 2021.
- [29] Y. Yan, M. Yang, H. Zhao, G. Duan, X. Peng, and J. Wang, "Drug repositioning based on multi-view learning with matrix completion," *Briefings in Bioinformatics*, vol. 23, no. 3, p. bbac054, 2022.
- [30] J. Ma, C. Li, Y. Zhang, Z. Wang, S. Li, Y. Guo, L. Zhang, H. Liu, X. Gao, and J. Song, "Mulga, a unified multi-view graph autoencoder-based approach for identifying drug–protein interaction and drug repositioning," *Bioinformatics*, vol. 39, no. 9, p. btad524, 2023.
- [31] Y. Hua, Z. Feng, X. Song, X.-J. Wu, and J. Kitterl, "Mmdg-dti: Drug–target interaction prediction via multimodal feature fusion and domain generalization," *Pattern Recognition*, vol. 157, p. 110887, 2025.
- [32] M. G. Rolf, J. O. Curwen, M. Veldman-Jones, C. Eberlein, J. Wang, A. Harmer, C. J. Hellowell, and M. Braddock, "In vitro pharmacological profiling of r406 identifies molecular targets underlying the clinical effects of fostamatinib," *Pharmacology research & perspectives*, vol. 3, no. 5, p. e00175, 2015.
- [33] P. Imming, C. Sinning, and A. Meyer, "Drugs, their targets and the nature and number of drug targets," *Nature reviews Drug discovery*, vol. 5, no. 10, pp. 821–834, 2006.
- [34] H. M. Berman, J. Westbrook, Z. Feng, G. Gilliland, T. N. Bhat, H. Weissig, I. N. Shindyalov, and P. E. Bourne, "The protein data bank," *Nucleic acids research*, vol. 28, no. 1, pp. 235–242, 2000.
- [35] A. Markham, "Brigatinib: first global approval," *Drugs*, vol. 77, pp. 1131–1135, 2017.
- [36] C. Haberler, E. Gelpi, C. Marosi, K. Rössler, P. Birner, H. Budka, and J. Hainfellner, "Immunohistochemical analysis of platelet-derived growth factor receptor- α - β , c-kit, c-abl, and arg proteins in glioblastoma: Possible implications for patient selection for imatinib mesylate therapy," *Journal of neuro-oncology*, vol. 76, pp. 105–109, 2006.
- [37] P. P. Piccaluga, S. Paolini, and G. Martinelli, "Tyrosine kinase inhibitors for the treatment of Philadelphia chromosome-positive adult acute lymphoblastic leukemia," *Cancer*, vol. 110, no. 6, pp. 1178–1186, 2007.
- [38] M. Amin, "American cancer society," *AJCC cancer staging manual. Eighth edition/editor-in-chief, Mahul B. Amin, MD, FACP*, vol. 1024, 2017.
- [39] E. Jabbour and H. Kantarjian, "Chronic myeloid leukemia: 2018 update on diagnosis, therapy and monitoring," *American journal of hematology*, vol. 93, no. 3, pp. 442–459, 2018.
- [40] C. G. Mullighan, C. B. Miller, I. Radtke, L. A. Phillips, J. Dalton, J. Ma, D. White, T. P. Hughes, M. M. Le Beau, C.-H. Pui *et al.*, "Bcr-abl1 lymphoblastic leukaemia is characterized by the deletion of ikaros," *Nature*, vol. 453, no. 7191, pp. 110–114, 2008.
- [41] K. K. Bhanumathy, A. Balagopal, F. S. Vizeacoumar, F. J. Vizeacoumar, A. Freywald, and V. Giambra, "Protein tyrosine kinases: their roles and their targeting in leukemia," *Cancers*, vol. 13, no. 2, p. 184, 2021.
- [42] Y.-F. Song, Y. Qu, X.-P. Cao, and W. Zhang, "Cellular localization of debromohymenialdisine and hymenialdisine in the marine sponge axinella sp. using a newly developed cell purification protocol," *Marine biotechnology*, vol. 13, pp. 868–882, 2011.
- [43] K. Huang, T. Fu, W. Gao, Y. Zhao, Y. Roohani, J. Leskovec, C. W. Coley, C. Xiao, J. Sun, and M. Zitnik, "Artificial intelligence foundation for therapeutic science," *Nature chemical biology*, vol. 18, no. 10, pp. 1033–1036, 2022.
- [44] G. Landrum, "RdKit: open-source cheminformatics from machine learning to chemical registration," in *Abstracts of Papers of the American Chemical Society*, vol. 258. AMER CHEMICAL SOC 1155 16TH ST, NW, WASHINGTON, DC 20036 USA, 2019.
- [45] J. L. Durant, B. A. Leland, D. R. Henry, and J. G. Nourse, "Reoptimization of mdl keys for use in drug discovery," *Journal of chemical information and computer sciences*, vol. 42, no. 6, pp. 1273–1280, 2002.
- [46] R. E. Carhart, D. H. Smith, and R. Venkataraghavan, "Atom pairs as molecular features in structure-activity studies: definition and applications," *Journal of Chemical Information and Computer Sciences*, vol. 25, no. 2, pp. 64–73, 1985.
- [47] H. L. Morgan, "The generation of a unique machine description for chemical structures—a technique developed at chemical abstracts service," *Journal of chemical documentation*, vol. 5, no. 2, pp. 107–113, 1965.
- [48] Z.-P. Feng and C.-T. Zhang, "Prediction of membrane protein types based on the hydrophobic index of amino acids," *Journal of protein chemistry*, vol. 19, pp. 269–275, 2000.
- [49] C. Cai, L. Han, Z. Ji, and Y. Chen, "Enzyme family classification by support vector machines," *Proteins: Structure, Function, and Bioinformatics*, vol. 55, no. 1, pp. 66–76, 2004.
- [50] K.-C. Chou, "Using amphiphilic pseudo amino acid composition to predict enzyme subfamily classes," *Bioinformatics*, vol. 21, no. 1, pp. 10–19, 2005.
- [51] J. Mukhoti, V. Kulharia, A. Sanyal, S. Golodetz, P. Torr, and P. Dokania, "Calibrating deep neural networks using focal loss," *Advances in neural information processing systems*, vol. 33, pp. 15 288–15 299, 2020.